**Versatile Synthetic Alternatives to Matrigel for Vascular Toxicity Screening and Stem Cell Expansion**

Eric H. Nguyen*[1,2,3], William T. Daly*[1,2,4], Ngoc Nhi T. Le[5], Mitra Farnoodian[3], David G. Belair[1,6], Michael P. Schwartz[1,7], Connie S. Lebakken[8], Gene E. Ananiev[9], Mohammad Ali Saghiri[3], Thomas B. Knudsen[6], Nader Sheibani[1,2,3], William L. Murphy[1,2,4,5]

*Co-first authorship - Both authors contributed equally to the work

1 Department of Biomedical Engineering, University of Wisconsin – Madison, WI, USA

2 Human Models for Analysis of Pathways (Human MAPs) Center, University of Wisconsin – Madison, WI, USA

3 Department of Ophthalmology and Visual Sciences, University of Wisconsin School of Medicine and Public Health, Madison, WI, USA

4 Department of Orthopedics and Rehabilitation, University of Wisconsin School of Medicine and Public Health, Madison, WI, USA

5 Materials Science Program, University of Wisconsin – Madison, WI, USA

6 U.S. Environmental Protection Agency (EPA), National Center for Computational Toxicology, Research Triangle Park, NC, USA

7 Center for Sustainable Nanotechnology, Department of Chemistry, University of Wisconsin – Madison, WI, USA

8 Stem Pharm, Inc., Madison, WI, USA

9 Small Molecule Screening Facility, University of Wisconsin – Madison, WI, USA

Disclaimer: The US Environmental Protection Agency, through its Office of Research and Development, funded and managed part of the research described here. The views expressed in this paper are those of the authors and do not necessarily reflect the views or policies of the US EPA

**SUPPLEMENTAL INFORMATION**

## Supplemental Introduction

### Alternative biomaterial arrays to modulate cell behavior

Synthetic and natural ECM arrays (ranging from 100s to 1000s of material combinations), presented as synthetic hydrogels[1-7], bioprinted 3D constucts[8], ceramics[9], different topographies or as biological/polymeric coatings of different substrates[10-15] have previously identified materials that can modulate cellular responses for *in vitro* and *in vivo* applications e.g. controlled expansion and differentiation of stem cells[4-6,9-14], maintenance of stem cell pluripotency[7], cardiomyocyte viability and maturation[8,10,16], bone formation and repair[15], and neural rosette formation[3].

### Rationale for using thiol-ene photocrosslinked hydrogels to modulate cell behavior

Hydrogel formulations using thiol-ene photocrosslinking chemistry and norbornene-functionalized PEG (PEG-NB) have previously been used in our lab for a broad number of applications. Examples include the controlled formation of vascularized multicellular cerebral neural assemblies[17], the enhanced differentiation of hESCs to neurons on more compliant/soft surfaces due to nuclear translocation of YAP to the cytoplasmic localization[18], the rapid formation of mature neural networks on the surface of the hydrogel with increased sensitivity to a botulinum neurotoxin [19], and the encapsulation of vascular networks both with or without microfluidic devices[20,21]. The synthetic hydrogels in these studies were functionalized and crosslinked using thiol-ene "click" photopolymerization. This method was chosen due to the consistent reaction kinetics of photopolymerization at ambient temperatures and pH. The reaction results in a 1:1 conversion rate of thiols to thio-esters, suggesting a high degree of specificity for reacting thiols to norbornene groups. Additionally, thiol-ene photopolymerization was performed at neutral, rather than alkaline pH, reducing the occurrence of disulfide bridge formation[22-26]. Ambient crosslinking conditions and spatiotemporal control of crosslinking are essential for generating large numbers of distinct hydrogels in array-based screening methods, such as those used to modulate stem cell behavior in past studies Based on our prior experience in array-based methods[6,16,27]. In contrast, other crosslinking chemistries, including the crosslinking of vinyl sulfone-functionalized PEG through Michael-type addition, are prone to generating disulfide bridges and are affected by the pH and temperature of the crosslinking environment[28,29]. The use of thiol-ene photopolymerization has consistently produced hydrogels with greater elastic moduli and lower swelling ratios[24,26,30] compared to hydrogels crosslinked using Michael-type addition[28,29]. This suggests that thiol-ene photopolymerization is more effective than Michael-type addition at

incorporating PEG and crosslinking molecules into hydrogel networks at expected stoichiometric ratios, thereby resulting in more mechanically robust hydrogels[26].

**Supplemental Results and Discussion**

**Evaluating crosslinking efficiency and long-term swelling properties of PEG hydrogels**

Hydrogel precursor solutions were evaluated for non-reacted thiol content before crosslinking, and hydrogel solutions showed minimal disulfide bridge formation among free thiols under storage as frozen solutions (Supp. Fig. 3A, B). The consumption of all available crosslinking molecules by the thiol-ene reaction as well as the incorporation of up to 70% of 8-arm PEG molecules into the hydrogel network (1.38 mM PEG out of 2 mM in precursor solution) after eight minutes UV exposure were also confirmed by the Ellman's assay and a PEGylated protein ELISA, respectively (Supp. Fig. 3C, D). After crosslinking, hydrogels were confirmed to be degradable by collagenase unless crosslinked using a 3.4 kDa dithiolated PEG crosslinking molecule (Supp. Fig. 4A). Additionally, hydrogels were confirmed to be stable up to two weeks of storage in phosphate buffered saline (1x PBS) at 2-8°C or 37ºC, as quantified using volumetric swelling ratio (Supp. Fig. 4B,C). Hydrogels crosslinked using MMP-degradable peptide did not demonstrate significant changes in swelling after one week of incubation in media at 37ºC, but saw significantly increased swelling after two weeks in incubation (far beyond the timeline of the vascular screening and stem cell expansion applications). Hydrogels crosslinked using dithiolated PEG crosslinking molecule did not demonstrate significant changes in swelling over two weeks of incubation in media at 37ºC (Supp. Fig. 4D). Finally, changes in incubation temperature between 2-8°C or 37ºC did not cause permanent changes in hydrogel stability, but rather reversible changes in volumetric swelling ratio (Supp. Fig. 4E).

**Comparing inhibitor activity on hydrogel arrays to prior studies in literature**

HUVEC networks on synthetic hydrogels demonstrated increased sensitivity to a number of known VEGF inhibitors in comparison to HUVEC networks on Matrigel, including Vatalanib®, Semaxanib®, Sunitinib®, and a soluble flt-1 (sFlt-1) receptor (Figure 3, Supp. Fig. 7A). In all of the above cases, the VEGF inhibitors demonstrated significant inhibition of network formation in a wider range of concentrations in the synthetic hydrogel-based assay compared to the Matrigel-based assay. Vatalanib® demonstrated inhibition at 2.5 – 20 μM concentrations on synthetic hydrogels, while inhibition was not detected Matrigel. In prior activity assays, Vatalanib® demonstrated dose dependent effects

on endothelial proliferation with an IC50 of 7 nM[31], inhibited tubule formation at 100 nM and 1 μM respectively and endothelial wound closure formation at 10 nM to 10 μM respectively. Semaxanib® demonstrated inhibition at 0.63 μM and 10-20 μM on synthetic hydrogels, while inhibition was not detected on Matrigel. In prior activity assays, Semaxanib® mediated inhibition was seen in 3-6 day HUVEC fibroblast co-cultures at 1 μM[32] and 10 μM[33]. In this instance, inhibition was detected across a broad range of doses in the synthetic hydrogel, without the addition of a supportive cellular layer and over a short time period (24-hour versus a five-day assay). Anti-VEGF did not demonstrate inhibition on synthetic hydrogels or Matrigel. Previous studies demonstrated mild to strong inhibition by 0.01 - 100 μg/ml anti-VEGF in alternative experimental setups[34-36]. The inability to detect the effects of anti-VEGF here may be attributed to the low concentrations of 8 ng/mL to 1 μg/ml anti-VEGF applied here, as well as the lack of supporting fibroblasts present in the tubulogenesis models. Sunitinib® demonstrated inhibition between concentrations 1.25 – 20 μM on the synthetic hydrogels, while inhibition was detected at 0.31 μM on Matrigel, and this effective concentration was subject to change significantly across technical replicates. Comparably, previous studies demonstrated inhibition as low as 0.1 μM in a seven-day HUVEC-fibroblast co-culture and 1 μM in a endothelial wound closure model[32]; inhibition was similarly demonstrated inhibition at 1 μM in breast tumor derived endothelial network formation assay[37]. However, demonstrations of inhibitory effects at lower doses have not been demonstrated in a tube formation assay without the addition of a supportive fibroblast layer where a 100 nM dose of Suntinib® was demonstrated to be effective.

**HUVEC sprouting in synthetic aortic ring sprouting assay**

When embedded in synthetic hydrogels and Matrigel, mouse aortic ring explants generated sprouting bodies over a period of seven days (Supp. Fig. 5). Inhibition by 300 nM Sunitinib was detected using an aortic ring sprouting assay in the current studies in both synthetic hydrogels and Matrigel, as quantified by a significant reduction in the number of sprouting bodies emerging from the aortic explants after seven days of culture (Supp. Fig. 5B). We demonstrated that aortic ring explants released sprouting bodies into surrounding synthetic hydrogels and Matrigel, an outcome that requires MMP activity (Supp. Fig. 5). Synthetic hydrogels may therefore be utilized as embedding substrates in organ culture systems or in organoid systems such as those in previous studies[3,17,38,39]. Future work will optimize the embedding protocol to enable sensitive detection of putative vascular inhibiting chemicals and differentiation between

invading mesenchymal cells and sprouting capillaries. However, this flexibility in applying the synthetic hydrogels enables multiple promising readouts of pVDC activity.

**Use of thiol-ene crosslinking chemistry to form PEG hydrogels**

The formation of completely ideal, stoichiometric networks has not been achieved using michael-type addition or thiol-ene photocrosslinking chemistry. The incomplete incorporation of all available PEG molecules into a hydrogel network is likely due to cyclization, or the reaction of a crosslinking molecule to multiple arms of a single PEG molecule rather than arms of separate PEG molecules. At the low 2 mM PEG monomer concentrations used in these studies, the non-inclusion of PEG molecules was expected and has been corroborated in prior literature[26]. Recently, enzymes such as Factor XIII have catalyzed PEG hydrogel crosslinking, and these have produced hydrogels with greater elastic moduli and lower equilibrium swelling ratios compared to hydrogels formed using thiol-ene photopolymerization[40-43]. While enzyme-catalyzed crosslinking procedures formed more ideal polymer networks, the reactions in those prior studies needed to be performed through the addition of Factor XIII, thrombin, $Ca^{2+}$, as well as the addition of multiple crosslinking moieties, one including Lysine and one including Glutamine in solution. Finally, the crosslinking reaction required reaction times of up to 1 hour to ensure complete crosslinking. These factors potentially increase the complexity of crosslinking procedures and sacrifice spatiotemporal control of hydrogel formation. As such, thiol-ene photopolymerization was chosen as the method to rapidly generate hydrogels for chemical screening. Ultimately, the results of our study demonstrate that we were able to reproducibly form hydrogels with a high degree of control. For example, Suppl. Figures 1 and 12 show ranges of elastic moduli that were reproducible across multiple studies using comparable hydrogel formulations[20,44,45].

**Impact of VEGF binding and sequestration in vascular inhibitory compound detection**

The synthetic hydrogels used in these studies were capable of modulating VEGF sequestration through the presentation of VBP, as demonstrated when VBP-functionalized hydrogels bound greater amounts of VEGF from surrounding media than hydrogels containing only RGD or scrambled VBP[46,47] (Supp. Fig. 2). In these studies, we leveraged VBP to investigate growth factor sequestration, often observed in natural extracellular matrices[46,48], as a potential mechanism behind the decreased sensitivity of the Matrigel-based angiogenesis assay to known VEGF inhibitors. Relative to angiogenesis assays performed on hydrogels that lacked VBP, assays performed on VBP-

functionalized hydrogels showed differential effects on assay sensitivity to VEGF inhibitors depending on whether they bind soluble VEGF (e.g. sflt-1) or inhibit VEGF receptor tyrosine kinase signaling (e.g. Vatalanib®). Based on our demonstration of VEGF sequestration by VBP-functionalized hydrogels, as well as binding characterization, observed binding of endogenous VEGF, and finite element modeling by Belair *et al*[47], we hypothesize that VEGF sequestration at the interface between hydrogels and media increases the local concentration of soluble exogenous and endogenous VEGF around endothelial cells. This possibly affects VEGF inhibitors in two ways: if VBP hydrogels concentrate VEGF locally to endothelial cells, the increased VEGF concentration would override the effects of inhibitors that bind soluble VEGF, such as anti-VEGF and sflt-1. In contrast, VBP can bind endogenous VEGF secreted by endothelial cells[49-51] and consequently decrease expression of VEGFR2, which is dependent on signaling by endogenous VEGF[52]. Decreased expression of VEGFR2 would increase cell sensitivity to receptor tyrosine kinase inhibitors such as Vatalanib®. Prinomastat HCl, a MMP inhibitor that acts independently of VEGF, did not see a decrease in activity due to the presence of VBP, suggesting that VBP specifically modulates VEGF signaling. The suggestion that growth factor sequestration changes the activity of growth factor-silencing compounds can motivate efforts to control sequestration in future toxicity assays in order to increase their sensitivity. Additional characterizations of VEGF-initiated signal transduction in the presence of VBP, such as characterizations of VEGFR2 phosphorylation and expression, ERK signaling, and MAPK activity[53], are required to confirm this hypothesis.

**Supplemental Methods**

**Characterization of hydrogel stability and non-crosslinked components**

To evaluate the availability of free thiol groups in hydrogel precursor solutions (Supp. Figure 3A), solutions containing 2 mM PEG, 0.125 mM cyclic RGD, 4 mM crosslinking peptide, (50% cross-linked) and 0.2% I2959 were analyzed using the Ellmans Assay (Thermo-Fisher) according to the manufacturer protocol, including with the use of a L-Cysteine hydrochloride standard curve. Solutions were aliquoted into amber tubes and frozen at -20°C for at least two hours prior to testing. Afterward, aliquots were thawed under cold running water and stored on ice prior to analysis. For freeze-thaw experiments, samples were re-frozen at -20 degrees for at least two hours prior to re-thawing. Several samples were also stored at 4°C, room temperature, and 37°C for 24 hours prior to analysis.

To evaluate the impact that disulfide bond formation has on the tubulogenesis assay (Supp. Figure 3B), precursor solutions containing 2 mM PEG, 0.125 mM cyclic RGD, 4 mM crosslinking peptide, (50% cross-linked) and 0.2%

I2959 were plated into 96-well Angiogenesis plates (Ibidi USA, Madison, WI) at a volume of 8 µL/well. The solutions were cured using 365 nm UV light at a 4.5 mW/cm$^2$ dose rate for 8 minutes. HUVECs, which were stained using Cell Tracker Red according to the standard protocol, were seeded at a density of 2.4 x $10^6$ cells/mL, treated with 0.2% DMSO per condition, and photographed after 24-hour incubation at 37°C.

To evaluate the concentration of non-reacted thiols extracted from cured synthetic hydrogels, precursor solutions containing 2 mM PEG, 0.125 mM cyclic RGD, and 4 mM crosslinking peptide (50% cross-linked) and 0.2% w/v I2959 were pipetted into the 24 well plates as 37.5 µL hydrogels and exposed to 365 nm UV light at a dose rate of 4.5 mW/cm$^2$ for 0, 5, 15, 20 or 480 seconds. The resulting hydrogels were bathed in 400 µL Ellman's Buffer and stored at room temperature for 90 minutes. The Ellman's buffer was removed and tested using the Ellman's Assay according to the manufacturer's protocol. Non-reacted thiol content was quantified as the concentration of free thiols remaining from the original precursor solution (Supp. Fig. 3C).

To evaluate the concentration of non-reacted PEG polymer extracted from cured synthetic hydrogels, precursor solutions characterized as containing 2 mM PEG, 0.125 mM cyclic RGD, 4 mM crosslinking peptide (50% cross-linked) and 0.2% I2959 were pipetted into the 24 well plates as 50 µL hydrogels and exposed to 365 nm UV light at a dose rate of 4.5 mW/cm$^2$ for 0, 5, 15, 20 or 480 seconds. The resulting hydrogels were bathed in 500 µL 1x PBS and stored at 37°C for 24 hours, after which 1x PBS was removed from the hydrogel, stored, and replaced with fresh 1x PBS. After an additional 24-hour incubation period, the 1x PBS was removed and stored. To evaluate the concentration of PEG polymer extracted from the hydrogels, the PBS taken from the hydrogels was tested using a PEGylated protein ELISA kit (Abcam, Cambridge, UK) according to the manufacturer's protocol, using 20 kDa, 8-arm PEGNB as a standard. Non-crosslinked PEG was quantified as the mass of PEG extracted from the hydrogels out of an expected value of 2 mM PEG per hydrogel (Supp, Fig. 3D).

To demonstrate the degradability of synthetic hydrogels used in endothelial network formation assays and non-degradability of hydrogels used in hESC expansion (Supp. Figure 4A), precursor solutions containing 2 mM PEG, 0.125 mM cyclic RGD, either 4 mM crosslinking peptide or dithiolated PEG crosslinker (50% cross-linked), and 0.2% w/v I2959 were pipetted into the cut ends of 1cc syringes (BD Biosciences) as 20 µL disks and exposed to 365 nm UV light for eight minutes at a dose rate of 4.5 mW/cm$^2$. The resulting hydrogels were ejected from the syringes into a 24 well plate containing 1 mL sterile 1x PBS and stored at 2-8°C for 24 hours. A pair of calipers was used to measure

the diameters and heights of the disks and evaluate the volumetric swelling ratio of the hydrogels. Afterward, 1x PBS was removed and replaced with 1x PBS containing 0, 10, or 100 µg/mL collagenase. The non-degradable hydrogels were treated with 1x PBS containing 100 µg/mL collagenase. The hydrogels were stored for an additional 24 hours at 37°C and measured again with calipers afterward. Swelling ratio was quantified as the volume of the hydrogels normalized to the original 20 µL volume.

To evaluate the stability of synthetic hydrogels stored at 2-8°C or 37°C (Supp. Figure 4B,C), precursor solutions containing 2 mM PEG, 0.125 mM cyclic RGD, 4 mM crosslinking peptide or dithiolated PEG crosslinker (50% cross-linked) and either 0.05 or 0.2% I2959 were pipetted into the cut ends of 1cc syringes (BD Biosciences) as 30 µL disks and exposed to 365 nm UV light at a dose rate of 4.5 mW/cm$^2$ for eight minutes. The resulting hydrogels were ejected from the syringes into a 24 well plate containing 1 mL sterile 1x PBS per well and stored at either 2-8°C or 37°C for two weeks. To evaluate changes in volumetric swelling ratio of the hydrogels over time, a pair of calipers was used to measure the diameters and heights of the disks 1, 2, 3 and 5 days after the start of incubation, then at 1 and 2-week time points. 1x PBS was exchanged after each measurement. Swelling ratio was quantified as the volume of the hydrogels normalized to the original 30 µL volume.

To evaluate the stability of synthetic hydrogels stored in media at 37°C (Supp. Figure 4D), precursor solutions containing 2 mM PEG, 0.125 mM cyclic RGD, 4 mM crosslinking peptide or dithiolated PEG crosslinker (50% cross-linked) and 0.2% I2959 were pipetted into the cut ends of 1cc syringes (BD Biosciences) as 30 µL disks and exposed to 365 nm UV light at a dose rate of 4.5 mW/cm$^2$ for eight minutes. The resulting hydrogels were ejected from the syringes into a 24 well plate containing 1mL sterile 1x PBS per well and incubated at 2-8°C for 24 hours. Afterward, 1x PBS was exchanged for 1 mL media per well and the hydrogels were incubated at 37°C for two weeks. Degradable hydrogels were incubated in Media 199 containing 3% Fetal Bovine Serum (Thermo Fisher Scientific, Inc., Carlsbad, CA), and non-degradable hydrogels were incubated in serum-free E8 basal medium (Life Technologies). To evaluate changes in volumetric swelling ratio of the hydrogels over time, a pair of calipers was used to measure the diameters and heights of the disks 1, 2, 3 and 5 days after hydrogel formation, then at 1 and 2-week time points. Media was exchanged after each measurement. Swelling ratio was quantified as the volume of the hydrogels normalized to the original 30 µL volume.

To evaluate whether changes in hydrogel swelling ratio due to incubation temperature was reversible or due to a permanent change in network structure (Supp. Figure 4E), precursor solutions containing 2 mM PEG, 0.125 mM cyclic RGD, 4 mM crosslinking peptide or dithiolated PEG crosslinker (50% cross-linked) and 0.2% I2959 were pipetted into the cut ends of 1cc syringes (BD Biosciences) as 30 µL disks and exposed to 365 nm UV light at a dose rate of 4.5 mW/cm$^2$ for 8 minutes. The resulting hydrogels were ejected from the syringes into a 24 well plate containing 1 mL sterile 1x PBS per well and stored at 2-8°C for 24 hours. Afterward, the samples were incubated at 37°C for 24 hours, then at 2-8°C for 24 hours. To evaluate changes in volumetric swelling ratio of the hydrogels over time, a pair of calipers was used to measure the diameters and heights of the disks every 24 hours. 1x PBS was exchanged after each measurement. Swelling ratio was quantified as the volume of the hydrogels normalized to the original 30 µL volume.

**Aortic ring ex vivo explant assay**

All experiments were carried in accordance with protocols approved by the University of Wisconsin Institutional Animal Care and Use Committee. Male wild-type Black 6 mice were obtained from Jackson Laboratories (Bar Harbor, ME) and from the laboratory of Olachi Mezu-Ndubuisi. Aorta from four 4-wk-old mice were dissected aseptically and stored in a 50-mL conical tube containing 40-mL ice-cold serum-free DMEM and washed by shaking the tube for 15 s. The periaortic fibro-adipose tissue was removed with microdissecting forceps and iridectomy scissors without damaging the aortic wall. One-millimeter-long aortic rings (8 per aorta) were sectioned and rinsed in three consecutive washes of DMEM. In Matrigel-based explant assays, the aorta sections were embedded in 12-well plates containing 0.3 mL Matrigel (10.8 mg/mL, BD Biosciences) with up to 4 sections per well. The Matrigel was then incubated at 31°C for 30 minutes to harden before 1 mL DMEM containing 1% FBS was added to each well. In PEG-based explant assays, the aorta sections were embedded in 12-well plates containing 0.5 mL hydrogel solution containing 2 mM PEG, 0.125 mM cyclic RGD, and 4 mM crosslinking peptide (50% cross-linked) and 0.05% w/v I2959, with up to 4 sections per well. The wells were exposed to 365 nm UV light for 2 minutes at a dose rate of 4.5 mW/cm$^2$ to solidify the hydrogels before 1 mL DMEM + 1% FBS was added to each well.

Explants were cultured for 24 hours before they were treated with 1 mL DMEM containing 1% FBS and 5 ng/mL rhVEGF (PeproTech, cat# 450-32, Rocky Hill, NJ). After 24 hours of VEGF stimulation, explants were cultured in 1 mL DMEM containing 1% FBS for 8 days, with media being exchanged every other day. Several conditions, which

were not randomized or blinded, were treated with 300 nM Sunitinib Malate added to media for 8 days. Eight-day cultures were photographed using a Nikon Eclipse TS-100 equipped with a Q Imaging 12 Bit Monocolor camera. Higher-resolution phase-contrast images were photographed using a Nikon TI-Eclipse microscope. Sprouting area was quantified as the number of sprouting bodies extending from the aortic ring explants. (Supp. Figure 5).

**List of Figures and Movies**

**Supplemental Figure 1 (A)** Shear modulus of synthetic hydrogels with varying PEG concentration and VBP presence in precursor solutions (n = 3). Characterization was performed twice over the course of these studies. (**B**) Synthetic hydrogels and Matrigel demonstrate the ability to form endothelial networks straight from cryopreservation that are sensitive to a known vascular inhibitor i.e. Sunitinib®. **-**, vehicle control. **+**, Sunitinib treatment (n = 6). The network formation test was performed twice over the course of these studies. (**C**) Fluorescent images demonstrating the ability of the hydrogels and matrigel to form vascular networks from routine culture and from cyropreservation and also vascular network disruption when exposed to 20 μM Sunitinib®. Data represents means and error bars represent standard deviations.

**Supplemental Figure 2 (A)** Hit conditions comprising 2 mM PEG, 0 – 0.25 mM RGD were tested in the thin-hydrogel screening system to identify HUVEC network-forming conditions which incorporated a VEGF binding peptide (VBP) into the formulation. The screen was performed once over the course of these studies. **(B)** The incorporation of 0.267 mM VBP into the optimal hydrogel formulation identified in (A) reduced the amount of freely available VEGF in the surrounding medium when compared to both scrambled peptide controls and blank hydrogel controls in a cell free experiment to evaluate VEGF binding (n = 3). This sequestration test was performed once over the course of these studies. *, $p < 0.05$, one-way ANOVA followed by post-hoc Tukey's Multiple Comparisons test. Data represents means and error bars represent standard deviations.

**Supplemental Figure 3** Characterization of synthetic hydrogel stability and non-crosslinked components. **(A)** Free thiol content in hydrogel precursor solutions was evaluated across multiple freeze-thaw cycles and following storage in multiple conditions (n = 3). *, $p < 0.05$ using a one-way ANOVA followed by post-hoc Dunnett's test compared to 1 freeze-thaw cycle. Data represents means and error bars represent standard deviations. **(B)** Functionality of hydrogels in the endothelial network formation assay was tested after precursor solutions were subjected to multiple freeze/thaw conditions or storage at various temperatures. Multiple freeze/thaw cycles resulted in minimal impact on the assay, while storage above freezing temperatures had a greater impact. **(C)** The concentration of non-reacted thiols removed from cured hydrogels was evaluated using the Ellmans Assay after precursor solutions were exposed to UV light for varying periods of time. Detected thiol levels, after consumption by disulfide formation during room temperature incubation, did not significantly decrease beyond 20 seconds of exposure, suggesting the consumption of all possible

crosslinking molecules by the thiol-ene reaction beyond 20 seconds of exposure (n = 3). Statistics were evaluated using a one-way ANOVA followed by post-hoc Tukey's Multiple Comparisons Test. Data represents means and error bars represent standard deviations. **(D)** The concentration of non-crosslinked PEG molecules removed from cured hydrogels, out of an expected 2 mM concentration contained in a precursor solution, was evaluated using a PEGylated protein ELISA kit. Non-crosslinked PEG was removed from the hydrogels and detected in 1x PBS, even in hydrogels cured for 480 seconds, suggesting that not all PEG molecules in the precursor solution are incorporated into the final hydrogel network (n = 3). Data represents means and error bars represent standard deviations. All tests were performed twice over the course of these studies.

**Supplemental Figure 4** Characterization of synthetic hydrogel swelling over time. **(A)** Degradation of synthetic hydrogels was evaluated as volumetric swelling ratio after 24-hour incubation in either 1x PBS, 1x PBS containing 10 µg/mL Collagenase I, or 1x PBS containing 100 µg/mL Collagenase I. Additionally, a non-degradable hydrogel, crosslinked using dithiolated PEG, was incubated in 1x PBS containing 100 µg/mL Collagenase I. Degradable hydrogels in 10 – 100 ug/ml collagenase dissolved during a 24-hour collagenase treatment (n = 3). **(B)** Degradable and non-degradable hydrogel stability, evaluated as volumetric swelling ratio, was measured over the course of two week of storage in sterile 1x PBS at 2-8°C and 37°C. Hydrogel swelling ratios did not significantly change over the course of two weeks (n = 3). Statistics were evaluated using a one-way ANOVA followed by post-hoc Dunnett's Test compared to the 24-hour timepoint. **(C)** Volumetric swelling ratios of degradable hydrogels, cured using either 0.05% or 0.2% w/v I2959 in solution, was measured over the course of two weeks of storage in sterile 1x PBS at 2-8°C and 37°C. Hydrogel swelling ratios did not significantly change over the course of two weeks (n = 3). Statistics were evaluated using a one-way ANOVA followed by post-hoc Dunnett's Test compared to the 24-hour timepoint. Additionally, photoinitiator concentration did not significantly change swelling ratios at any time point. This was evaluated using a one-way ANOVA followed by Tukey's Multiple Comparisons test ($P < 0.05$). **(D)** Degradable and non-degradable hydrogel stability, evaluated as volumetric swelling ratio, was measured over the course of two weeks of storage in M199 + 3% fetal bovine serum (vascular screening PEG formulation) or E8 basal medium (stem cell expansion formulation), respectively, at 37°C. Swelling ratios of MMP-degradable hydrogels significantly increased after two weeks of incubation, while swelling ratios of non-degradable hydrogels did not significantly change over the course of 2 weeks (n = 3). Statistics were evaluated using a one-way ANOVA followed by post-hoc Dunnett's Test compared to the 48-hour timepoint (*, $p < 0.05$). **(E)** Reversibility of degradable and non-degradable hydrogel

volumetric swelling ratios with changing incubation temperatures. Hydrogels were incubated at 2-8°C for 24 hours. Afterward, the samples were incubated at 37°C for 24 hours, then at 2-8°C for 24 hours to determine if temperature-dependent changes in swelling ratios were reversible or due to permanent degradation of the polymer network ($n = 3$). Statistics were evaluated using a one-way ANOVA followed by post-hoc Dunnett's Test compared to the 24-hour timepoint (*, $p < 0.05$). All tests were performed twice over the course of these studies.

**Supplemental Figure 5** Aortic explant sprouting assays in Matrigel and synthetic hydrogels. **(A)** Brightfield micrographs comparing sprout emergence (arrowheads) from mouse aortic explants in Matrigel and synthetic hydrogels (n=4 per condition). Photographs were taken for quantification after 7 days of culture. **(B)** Number of sprouts emerging from aortic explants embedded in Matrigel and synthetic hydrogels. Sprouting number was quantified as the number of elongated structures still attached to the aortic explant (n=4 per condition, results pooled from two technical replicates. Non-sprouting DMSO-treated explants were excluded from quantification. *, $p < 0.05$ between DMSO controls and treatment with 300 nM Sunitinib, one-way ANOVA followed by post-hoc Tukey's multiple comparisons test). Data represents means and error bars represent standard deviations. The aortic ring ex vivo sprouting experiments were performed twice over the course of these studies.

**Supplemental Figure 6** Synthetic PEG hydrogels optimized for use in 96-well angiogenesis plates. Arrowheads indicate parameters used in inhibitor screening studies. **(A)** Dependence of hydrogel swelling ratio on photoinitiator concentration in the hydrogels. Swelling ratio was taken as ratio of sample diameter compared to the 3.5 mm diameter of the biopsy punch that extracted the samples. Columns in each photoinitiator condition represent swelling ratios measured in the individual rows of the 96 well plate to indicate spatial effects on swelling ratio ($n = 3$). *, &, $p < 0.05$ compared to rows A and H, respectively, Student's two-tailed T-test. This test was performed twice over the course of these studies. Data represents means and error bars represent standard deviations. **(B)** Identifying hydrogel volumes that minimize meniscus formation and the appearance of out-of-focus areas in network images. This test was performed once over the course of these studies. **(C)** Identifying cell seeding densities that result in interconnected endothelial networks. This test was performed once over the course of these studies. Red: Cell Tracker Red.

**Supplemental Figure 7** Fluorescent micrographs comparing HUVEC networks on synthetic hydrogel and Matrigel systems. Endothelial cells were treated with inhibitors to **(A)** VEGF signaling and **(B)** Prinomastat HCl as an inhibitor to MMP activity. In most cases, VEGF inhibitors show significant interference with network disruption on synthetic

hydrogels but not Matrigel at most tested inhibitor concentrations. Prinomastat HCl disrupts endothelial network formation on synthetic hydrogels at all treatment concentrations but permits network formation on Matrigel at multiple concentrations. Red: Cell Tracker Red.

**Supplemental Figure 8** Fluorescent micrographs comparing inhibitor-treated HUVEC networks on VBP-functionalized hydrogels. **(A)** Schematic of ideal synthetic hydrogels lacking or containing VBP. **(B)** The presence of VBP in hydrogels nullify effects of sflt-1 and increases cell sensitivity to Vatalanib®. Red: Cell Tracker Red.

**Supplemental Figure 9** HUVEC network formation following treatment with known VEGF inhibitory compounds. Any changes to network formation that are detectable on synthetic hydrogels fall into four qualitative categories. Inhibition by low doses of SU5416 results in the formation of disconnected networks. Inhibition by soluble Flt-1 enables broadening of network structures and increased network area. Inhibition by Sunitinib results in disruption of cell-cell contacts and rounded morphology of HUVECs. Protease inhibition by Prinomastat HCl results in the formation of cell monolayers rather than endothelial cell networks.

**Supplemental Figure 10** Fluorescent micrographs comparing Suramin-treated HUVEC networks on synthetic hydrogels and Matrigel. Suramin dissolves the Matrigel substrate at concentrations of 70 μM and 17.5 μM. Identical concentrations of Suramin on the synthetic hydrogels have little to no effect on endothelial network morphology and do not compromise substrate integrity to the same degree as on Matrigel. Red: Cell Tracker Red.

**Supplemental Figure 11** Examples of compounds identified as inhibitors by either the synthetic or Matrigel systems but not in both systems. **(A)** Inhibitors in the blinded sample matrix of 38 compounds identified on synthetic hydrogels, Matrigel, or both materials. **(B)** Sample images highlighting differential effects of inhibitors on synthetic hydrogels and Matrigel. Red: Cell Tracker Red.

**Supplemental Figure 12** Shear modulus of synthetic hydrogels used in hESC culture. Variables included 20 kDa PEG concentration and crosslinking percentage by 3.4 kDa dithiolated PEG crosslinking molecules in the precursor solutions (n = 3). Data represents means and error bars represent standard deviations. This characterization was performed once over the course of these studies.

**Supplemental Figure 13** Material-dependent maintenance of hESC pluripotency. Quantitative heat map of hESC NANOG, OCT3/4 and SOX-2 expression in a subset of synthetic hydrogel-based culture conditions screened in Figure

5. (n=3, n=5 in colony seeding conditions where ROCK inhibitor was removed, n=10 in single-cell seeding conditions where ROCK inhibitor was removed). Cells were cultured with either 0 or 5 μM ROCK inhibitor in maintenance culture, and hydrogels contained 0, 1, 2 or 4 mM cyclic RGD. The screen was performed once over the course of these studies.

**Supplemental Figure 14** NMR quantification of peptide conjugation to PEG molecules, as performed after each conjugation reaction. **(A)** Functionalization of available PEG arms with norbornene groups was quantified through integration of proton peaks between 6.8-7.2 PPM, representing alkene protons present on a norbornene ring. After conjugation with a peptide, a reduction in alkene protons is seen, indicating that norbornene groups have been consumed by the thiol-ene reaction (n = 1 per characterization). **(B)** The number of arms of each PEG molecule is calculated through the difference between the % norbornene molecule functionalization of unreacted and reacted PEG molecules (n = 1 per characterization).

**Supplemental Movie 1** Endothelial network formation by HUVECs over the course of 24 hours after seeding onto PEG Hydrogels.

**Supplemental Movie 2** Endothelial network formation by HUVECs over the course of 24 hours after seeding onto Matrigel.

**Supplemental Movie 3** Endothelial network formation by iPSC-ECs over the course of 24 hours after seeding onto PEG Hydrogels.

**Supplemental Movie 4** Process of thin hydrogel array formation.

**Supplemental Figures and Movies**

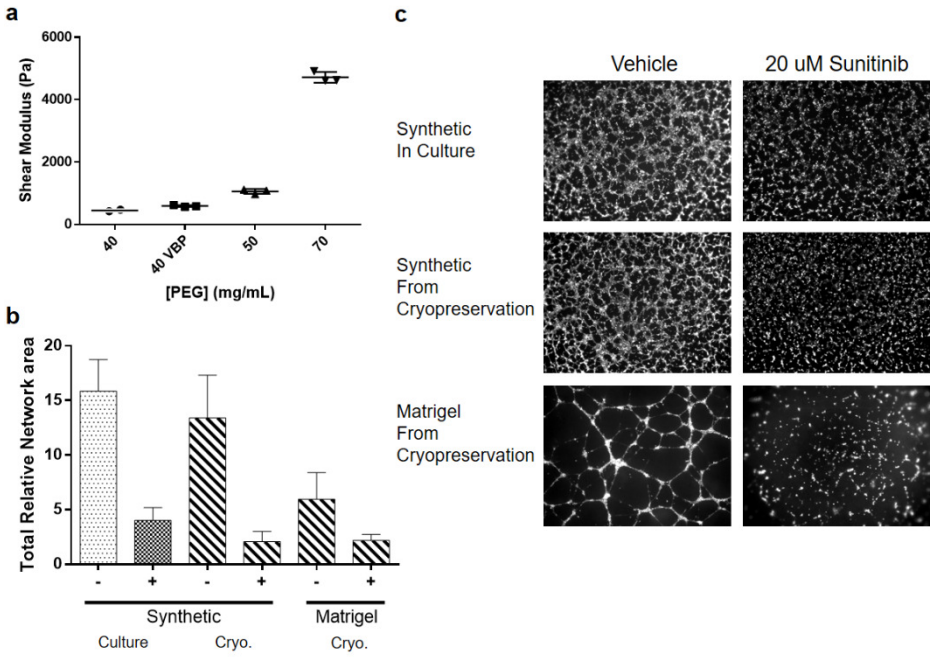


**Supplemental Figure 1 (A)** Shear modulus of synthetic hydrogels with varying PEG concentration and VBP presence in precursor solutions (n = 3). Characterization was performed twice over the course of these studies. (**B**) Synthetic hydrogels and Matrigel demonstrate the ability to form endothelial networks straight from cryopreservation that are sensitive to a known vascular inhibitor i.e. Sunitinib®. **-**, vehicle control. **+**, Sunitinib treatment (n = 6). The network formation test was performed once over the course of these studies. (**C**) Fluorescent images demonstrating the ability of the hydrogels and matrigel to form vascular networks from routine culture and from cyropreservation and also vascular network disruption when exposed to 20 µM Sunitinib®. Data represents means and error bars represent standard deviations.

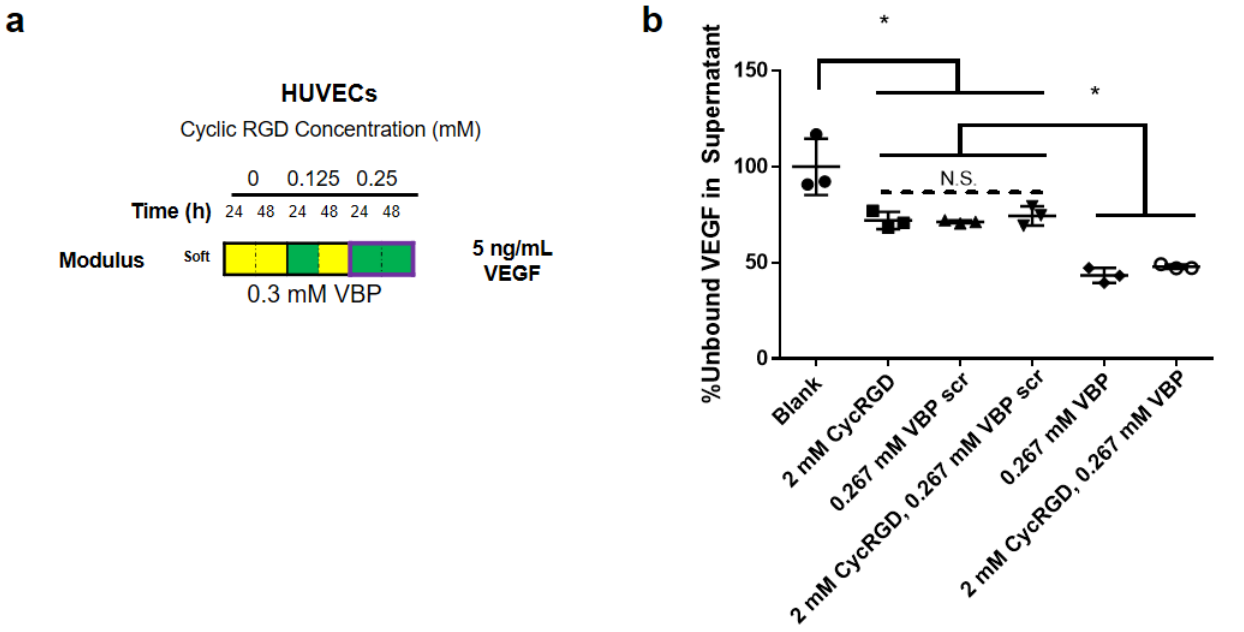


**Supplemental Figure 2 (A)** Hit conditions comprising 2 mM PEG, 0 – 0.25 mM RGD were tested in the thin-hydrogel screening system to identify HUVEC network-forming conditions which incorporated a VEGF binding peptide (VBP) into the formulation. The screen was performed once over the course of these studies. **(B)** The incorporation of 0.267 mM VBP into the optimal hydrogel formulation identified in (A) reduced the amount of freely available VEGF in the surrounding medium when compared to both scrambled peptide controls and blank hydrogel controls in a cell free experiment to evaluate VEGF binding (n = 3). This sequestration test was performed once over the course of these studies. *, $p < 0.05$, one-way ANOVA followed by post-hoc Tukey's Multiple Comparisons test. Data represents means and error bars represent standard deviations.

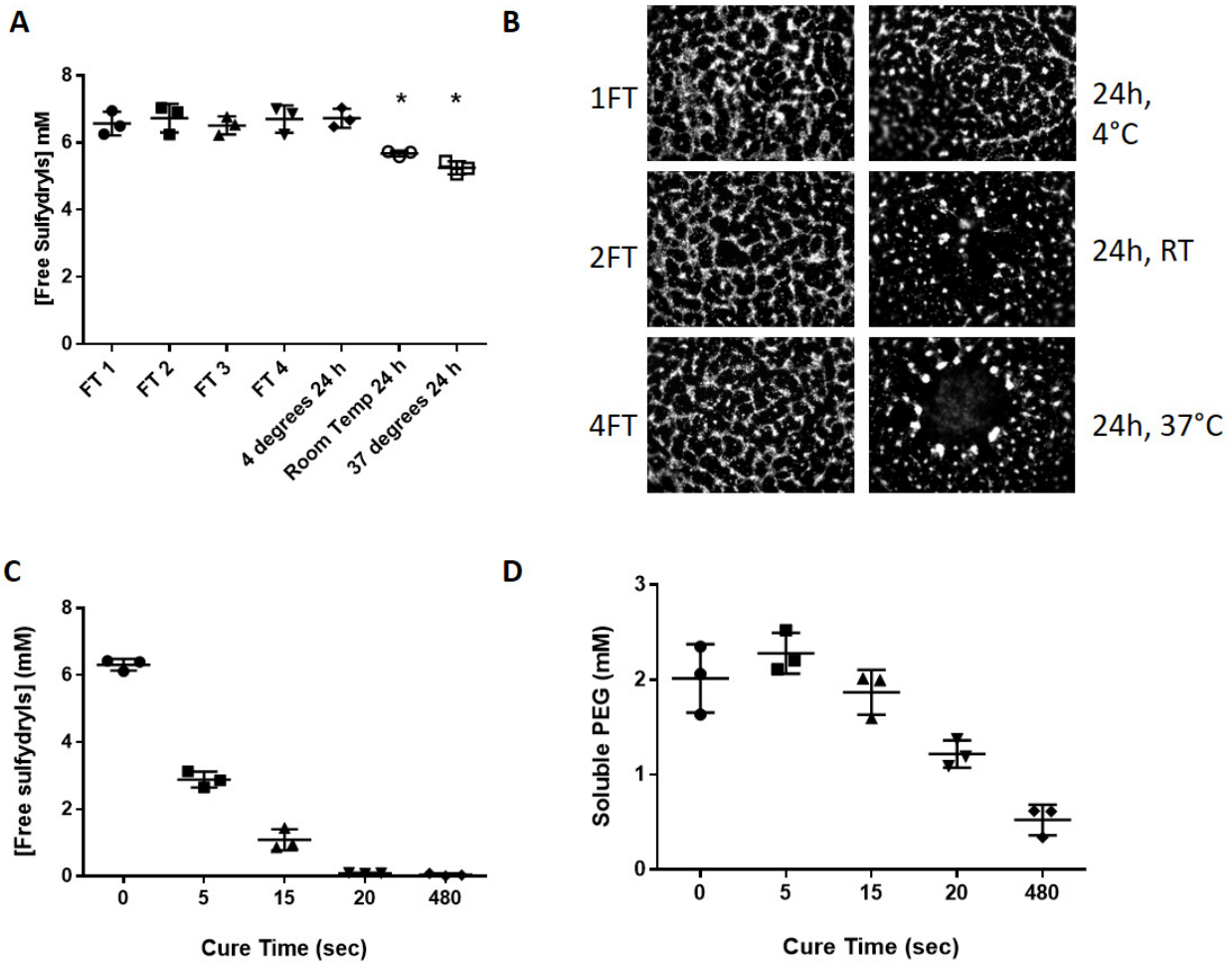


**Supplemental Figure 3** Characterization of synthetic hydrogel stability and non-crosslinked components. **(A)** Free thiol content in hydrogel precursor solutions was evaluated across multiple freeze-thaw cycles and following storage in multiple conditions (n = 3). *, $p < 0.05$ using a one-way ANOVA followed by post-hoc Dunnett's test compared to 1 freeze-thaw cycle. Data represents means and error bars represent standard deviations. **(B)** Functionality of hydrogels in the endothelial network formation assay was tested after precursor solutions were subjected to multiple freeze/thaw conditions or storage at various temperatures. Multiple freeze/thaw cycles resulted in minimal impact on the assay, while storage above freezing temperatures had a greater impact. **(C)** The concentration of non-reacted thiols removed from cured hydrogels was evaluated using the Ellmans Assay after precursor solutions were exposed to UV light for varying periods of time. Detected thiol levels, after consumption by disulfide formation during room temperature incubation, did not significantly decrease beyond 20 seconds of exposure, suggesting the consumption of all possible crosslinking molecules by the thiol-ene reaction beyond 20 seconds of exposure (n = 3). Statistics were evaluated

using a one-way ANOVA followed by post-hoc Tukey's Multiple Comparisons Test. Data represents means and error bars represent standard deviations. **(D)** The concentration of non-crosslinked PEG molecules removed from cured hydrogels, out of an expected 2 mM concentration contained in a precursor solution, was evaluated using a PEGylated protein ELISA kit. Non-crosslinked PEG was removed from the hydrogels and detected in 1x PBS, even in hydrogels cured for 480 seconds, suggesting that not all PEG molecules in the precursor solution are incorporated into the final hydrogel network (n = 3). Data represents means and error bars represent standard deviations. All tests were performed twice over the course of these studies.

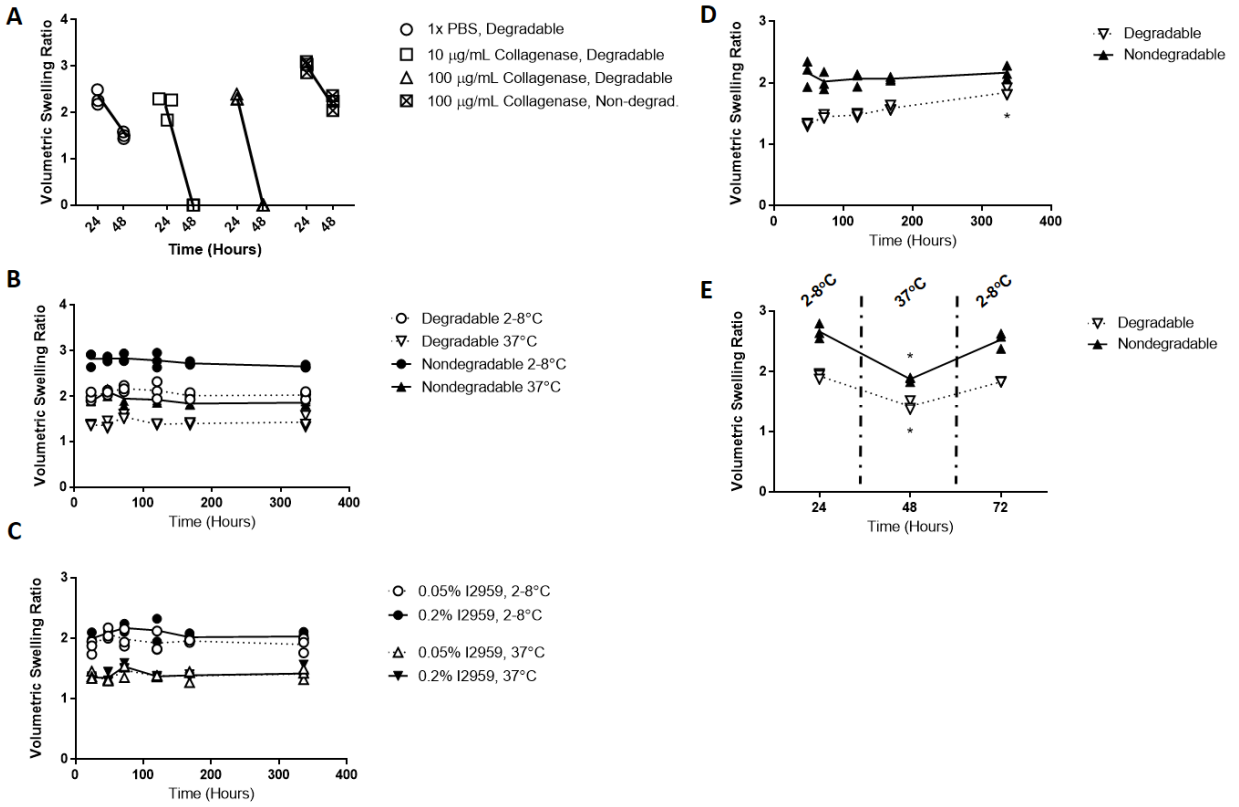


**Supplemental Figure 4** Characterization of synthetic hydrogel swelling over time. **(A)** Degradation of synthetic hydrogels was evaluated as volumetric swelling ratio after 24-hour incubation in either 1x PBS, 1x PBS containing 10 µg/mL Collagenase I, or 1x PBS containing 100 µg/mL Collagenase I. Additionally, a non-degradable hydrogel, crosslinked using dithiolated PEG, was incubated in 1x PBS containing 100 µg/mL Collagenase I. Degradable hydrogels in 10 – 100 ug/ml collagenase dissolved during a 24-hour collagenase treatment (n = 3). **(B)** Degradable and non-degradable hydrogel stability, evaluated as volumetric swelling ratio, was measured over the course of two week of storage in sterile 1x PBS at 2-8°C and 37°C. Hydrogel swelling ratios did not significantly change over the course of two weeks (n = 3). Statistics were evaluated using a one-way ANOVA followed by post-hoc Dunnett's Test compared to the 24-hour timepoint. **(C)** Volumetric swelling ratios of degradable hydrogels, cured using either 0.05% or 0.2% w/v I2959 in solution, was measured over the course of two weeks of storage in sterile 1x PBS at 2-8°C and 37°C. Hydrogel swelling ratios did not significantly change over the course of two weeks (n = 3). Statistics were evaluated using a one-way ANOVA followed by post-hoc Dunnett's Test compared to the 24-hour timepoint. Additionally, photoinitiator concentration did not significantly change swelling ratios at any time point. This was evaluated using a one-way ANOVA followed by Tukey's Multiple Comparisons test ($P < 0.05$). **(D)** Degradable and

non-degradable hydrogel stability, evaluated as volumetric swelling ratio, was measured over the course of two weeks of storage in M199 + 3% fetal bovine serum (vascular screening PEG formulation) or E8 basal medium (stem cell expansion formulation), respectively, at 37°C. Swelling ratios of MMP-degradable hydrogels significantly increased after two weeks of incubation, while swelling ratios of non-degradable hydrogels did not significantly change over the course of 2 weeks (n = 3). Statistics were evaluated using a one-way ANOVA followed by post-hoc Dunnett's Test compared to the 48-hour timepoint (*, $p < 0.05$). **(E)** Reversibility of degradable and non-degradable hydrogel volumetric swelling ratios with changing incubation temperatures. Hydrogels were incubated at 2-8°C for 24 hours. Afterward, the samples were incubated at 37°C for 24 hours, then at 2-8°C for 24 hours to determine if temperature-dependent changes in swelling ratios were reversible or due to permanent degradation of the polymer network (n = 3). Statistics were evaluated using a one-way ANOVA followed by post-hoc Dunnett's Test compared to the 24-hour timepoint (*, $p < 0.05$). All tests were performed twice over the course of these studies.

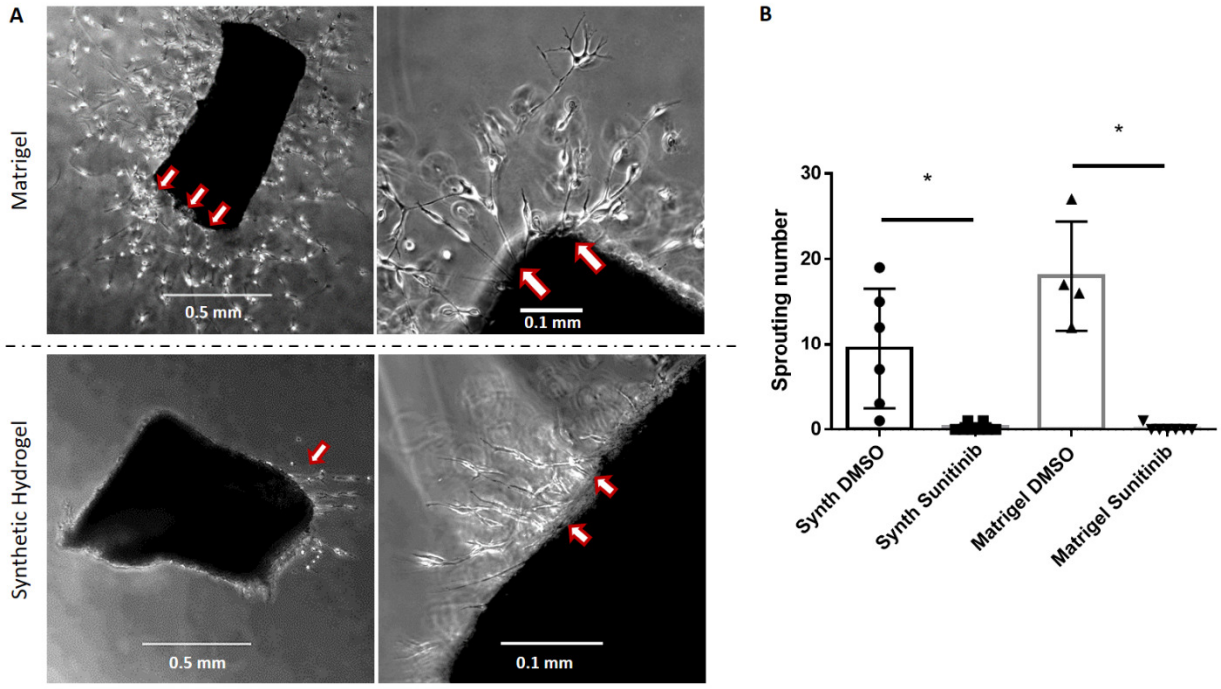


**Supplemental Figure 5** Aortic explant sprouting assays in Matrigel and synthetic hydrogels. **(A)** Brightfield micrographs comparing sprout emergence (arrowheads) from mouse aortic explants in Matrigel and synthetic hydrogels (n=4 per condition). Photographs were taken for quantification after 7 days of culture. **(B)** Number of sprouts emerging from aortic explants embedded in Matrigel and synthetic hydrogels. Sprouting number was quantified as the number of elongated structures still attached to the aortic explant (n=4 per condition, results pooled from two technical replicates. Non-sprouting DMSO-treated explants were excluded from quantification. *, $p < 0.05$ between DMSO controls and treatment with 300 nM Sunitinib, one-way ANOVA followed by post-hoc Tukey's multiple comparisons test). Data represents means and error bars represent standard deviations. The aortic ring ex vivo sprouting experiments were performed twice over the course of these studies.

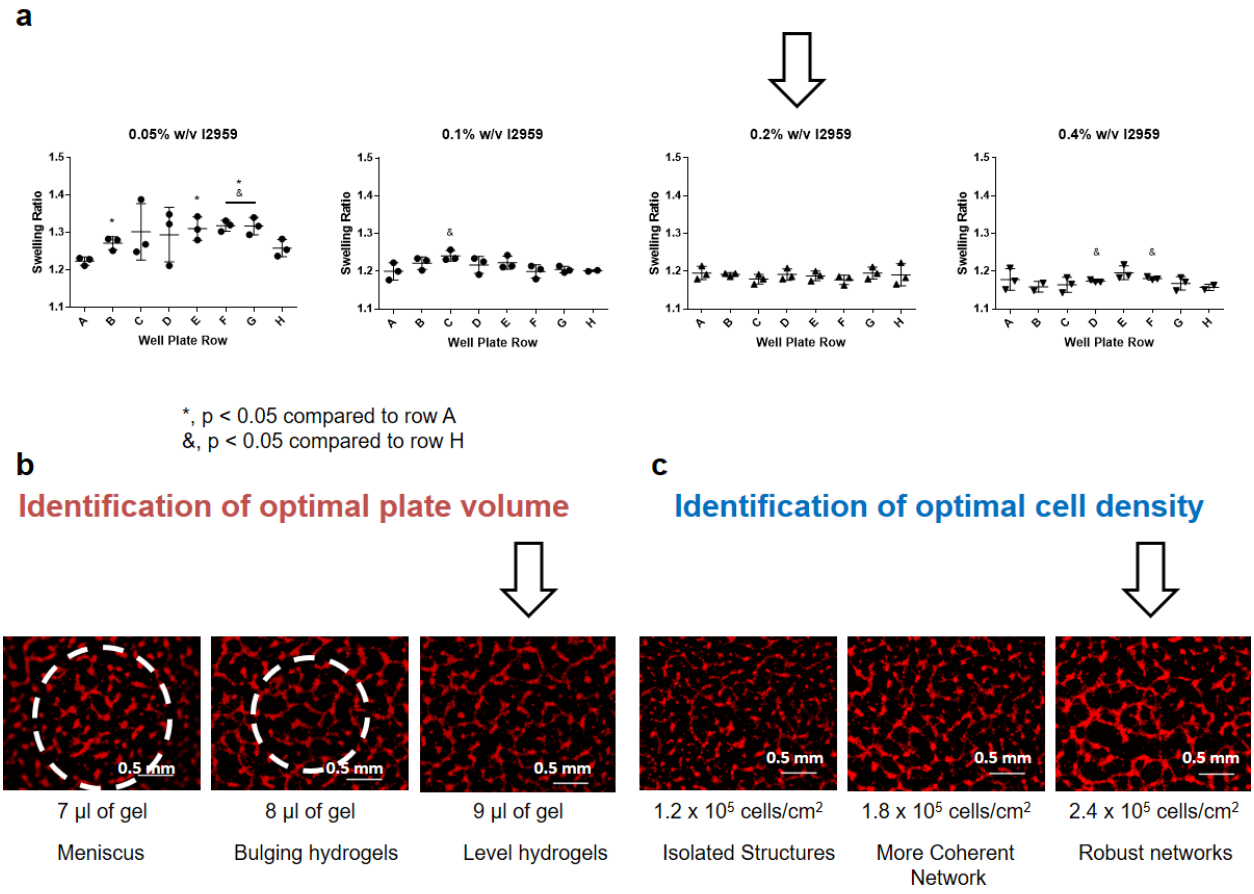


**Supplemental Figure 6** Synthetic PEG hydrogels optimized for use in 96-well angiogenesis plates. Arrowheads indicate parameters used in inhibitor screening studies. **(A)** Dependence of hydrogel swelling ratio on photoinitiator concentration in the hydrogels. Swelling ratio was taken as ratio of sample diameter compared to the 3.5 mm diameter of the biopsy punch that extracted the samples. Columns in each photoinitiator condition represent swelling ratios measured in the individual rows of the 96 well plate to indicate spatial effects on swelling ratio (n = 3). *, &, $p < 0.05$ compared to rows A and H, respectively, Student's two-tailed T-test. This test was performed twice over the course of these studies. Data represents means and error bars represent standard deviations. **(B)** Identifying hydrogel volumes that minimize meniscus formation and the appearance of out-of-focus areas in network images. This test was performed once over the course of these studies. **(C)** Identifying cell seeding densities that result in interconnected endothelial networks. This test was performed once over the course of these studies. Red: Cell Tracker Red.

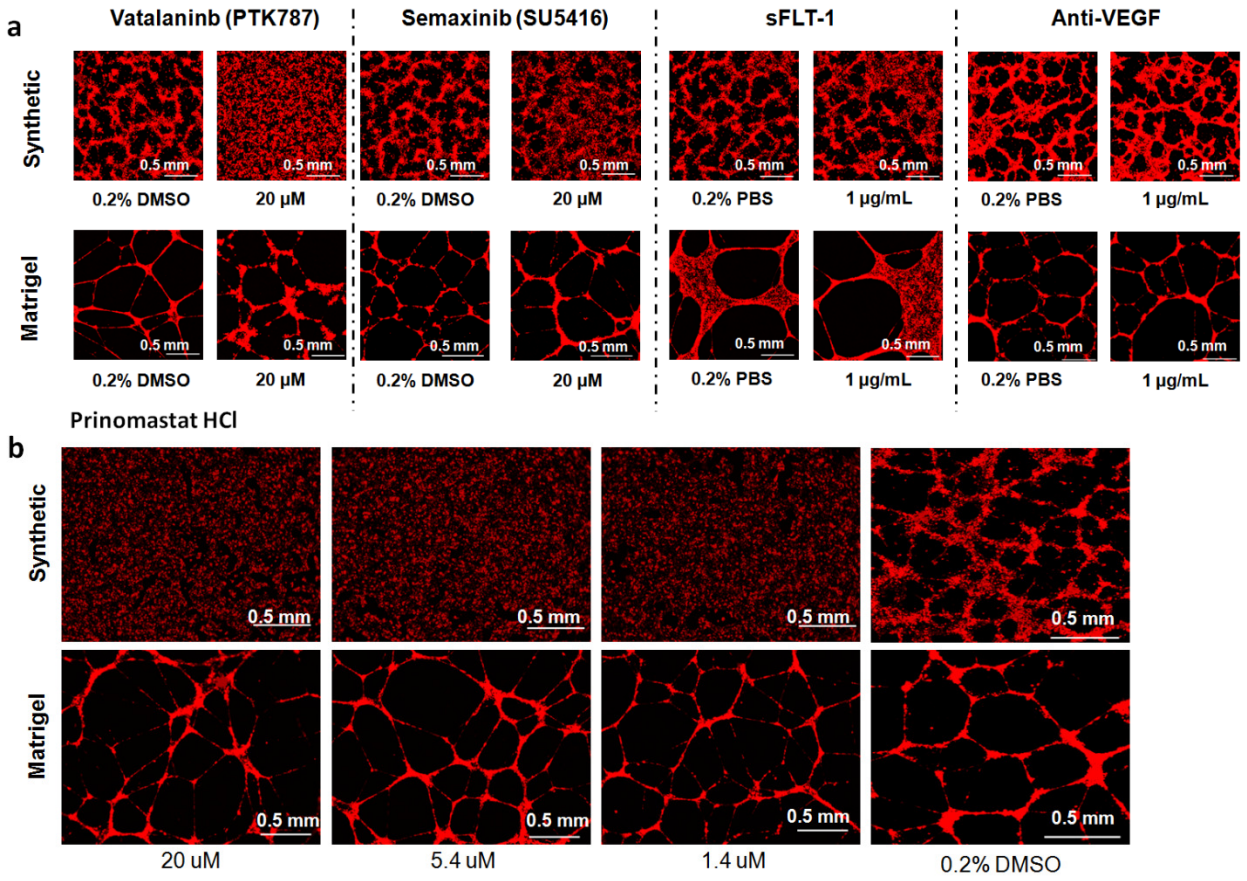


**Supplemental Figure 7** Fluorescent micrographs comparing HUVEC networks on synthetic hydrogel and Matrigel systems. Endothelial cells were treated with inhibitors to **(A)** VEGF signaling and **(B)** Prinomastat HCl as an inhibitor to MMP activity. In most cases, VEGF inhibitors show significant interference with network disruption on synthetic hydrogels but not Matrigel at most tested inhibitor concentrations. Prinomastat HCl disrupts endothelial network formation on synthetic hydrogels at all treatment concentrations but permits network formation on Matrigel at multiple concentrations. Red: Cell Tracker Red.

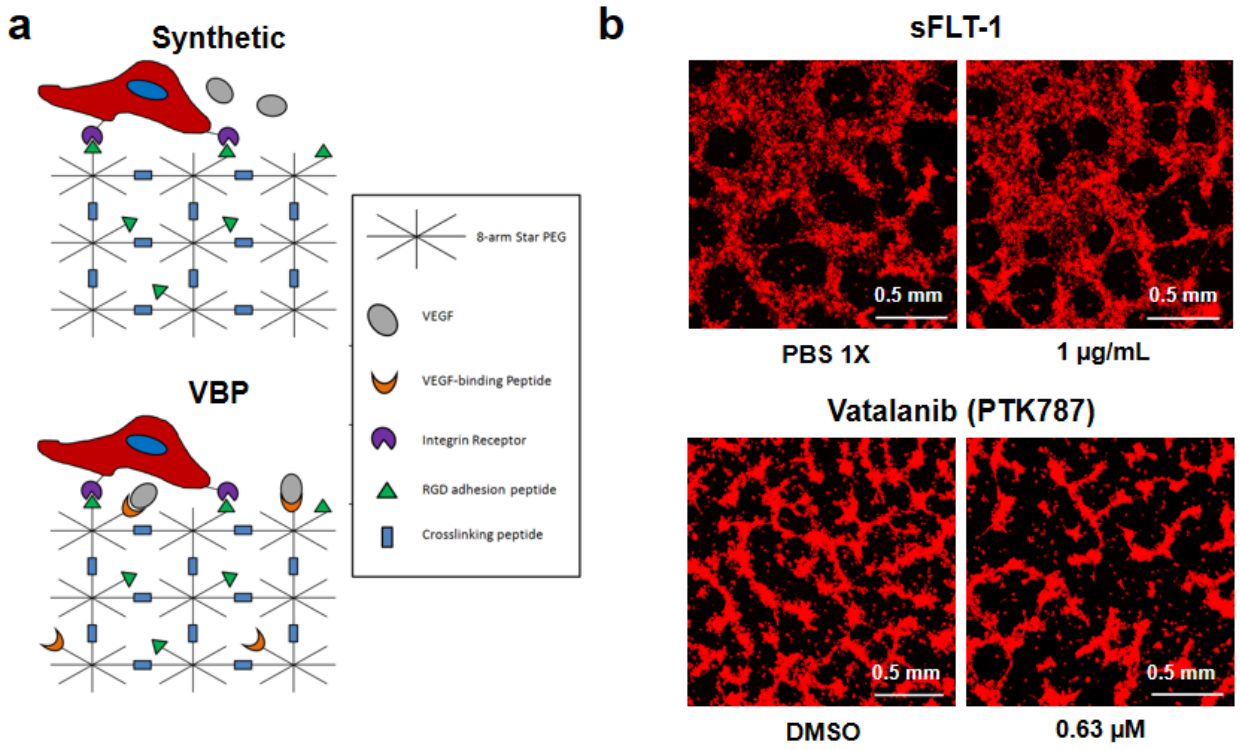


**Supplemental Figure 8** Fluorescent micrographs comparing inhibitor-treated HUVEC networks on VBP-functionalized hydrogels. **(A)** Schematic of ideal synthetic hydrogels lacking or containing VBP. **(B)** The presence of VBP in hydrogels nullify effects of sflt-1 and increases cell sensitivity to Vatalanib®. Red: Cell Tracker Red.

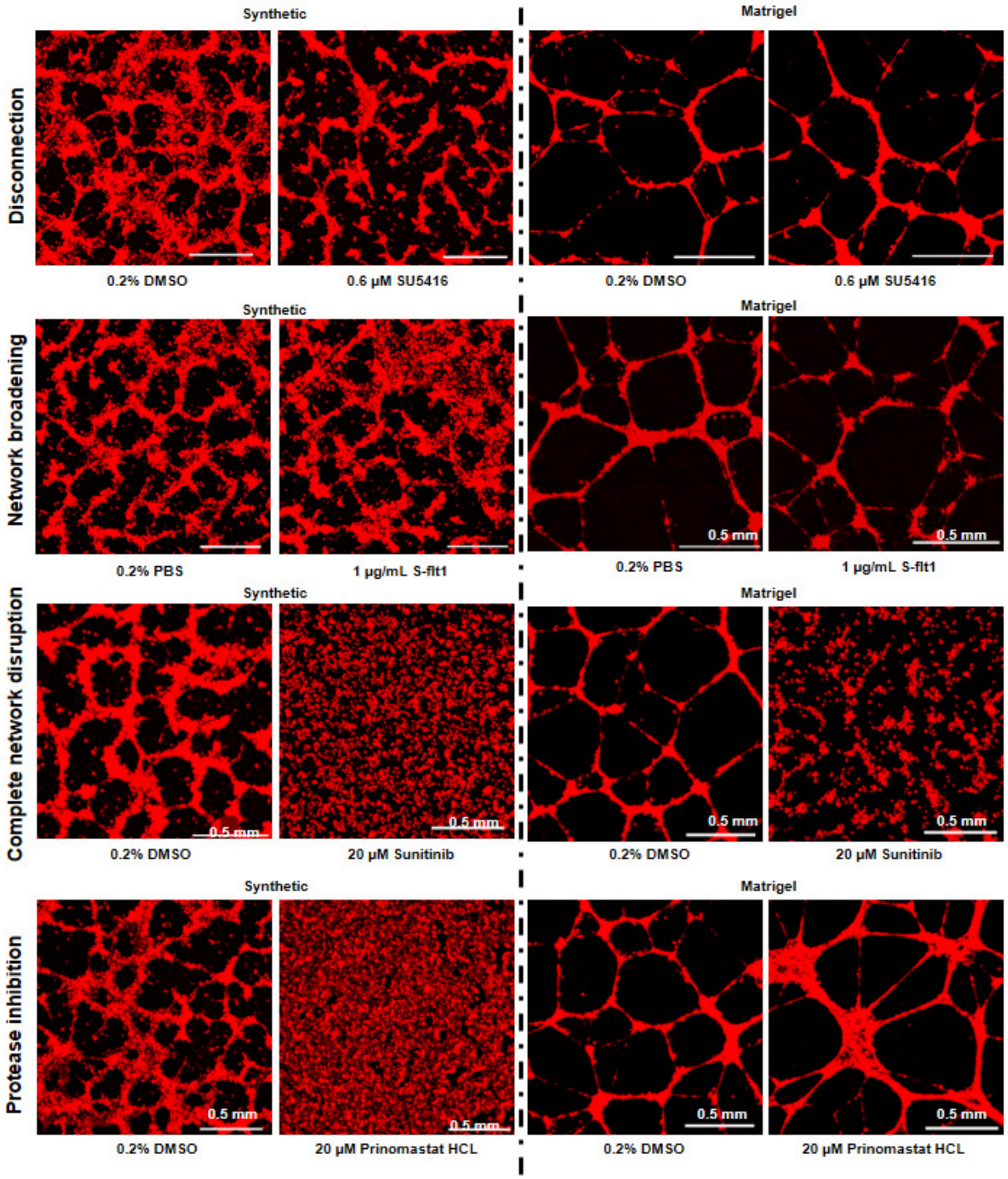


**Supplemental Figure 9** HUVEC network formation following treatment with known VEGF inhibitory compounds. Any changes to network formation that are detectable on synthetic hydrogels fall into four qualitative categories. Inhibition by low doses of SU5416 results in the formation of disconnected networks. Inhibition by soluble Flt-1 enables broadening of network structures and increased network area. Inhibition by Sunitinib results in disruption of

cell-cell contacts and rounded morphology of HUVECs. Protease inhibition by Prinomastat HCl results in the formation of cell monolayers rather than endothelial cell networks.

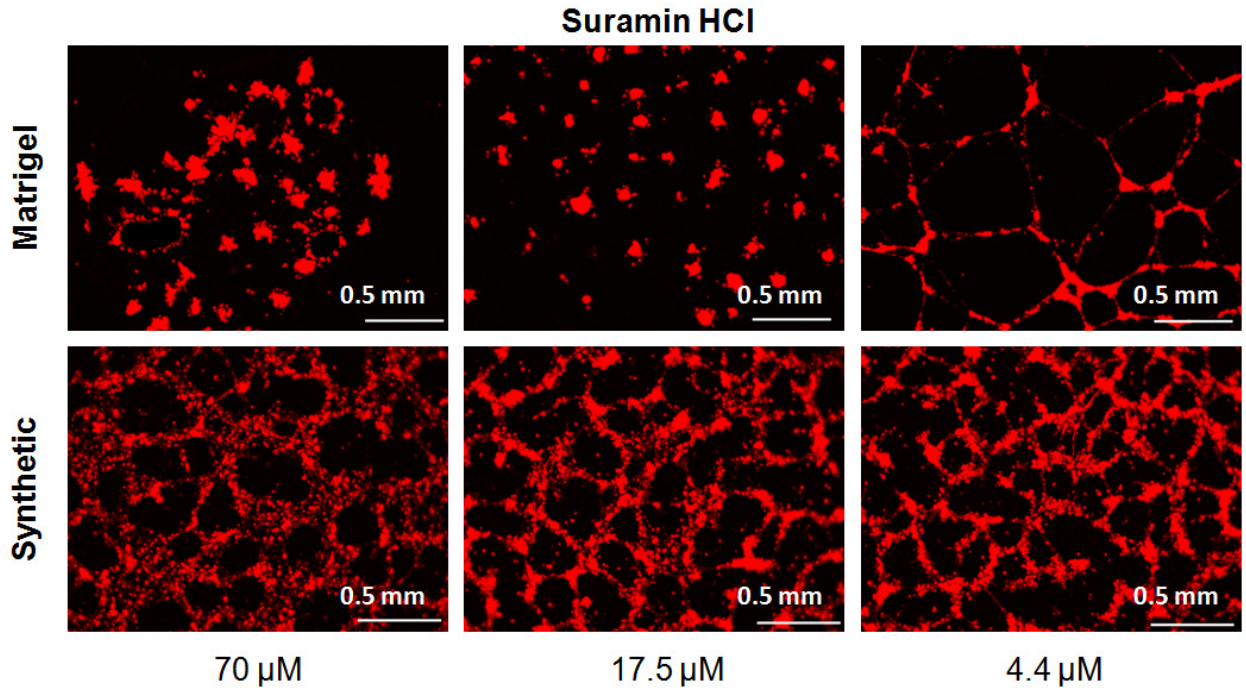


**Supplemental Figure 10** Fluorescent micrographs comparing Suramin-treated HUVEC networks on synthetic hydrogels and Matrigel. Suramin dissolves the Matrigel substrate at concentrations of 70 µM and 17.5 µM. Identical concentrations of Suramin on the synthetic hydrogels have little to no effect on endothelial network morphology and do not compromise substrate integrity to the same degree as on Matrigel. Red: Cell Tracker Red.

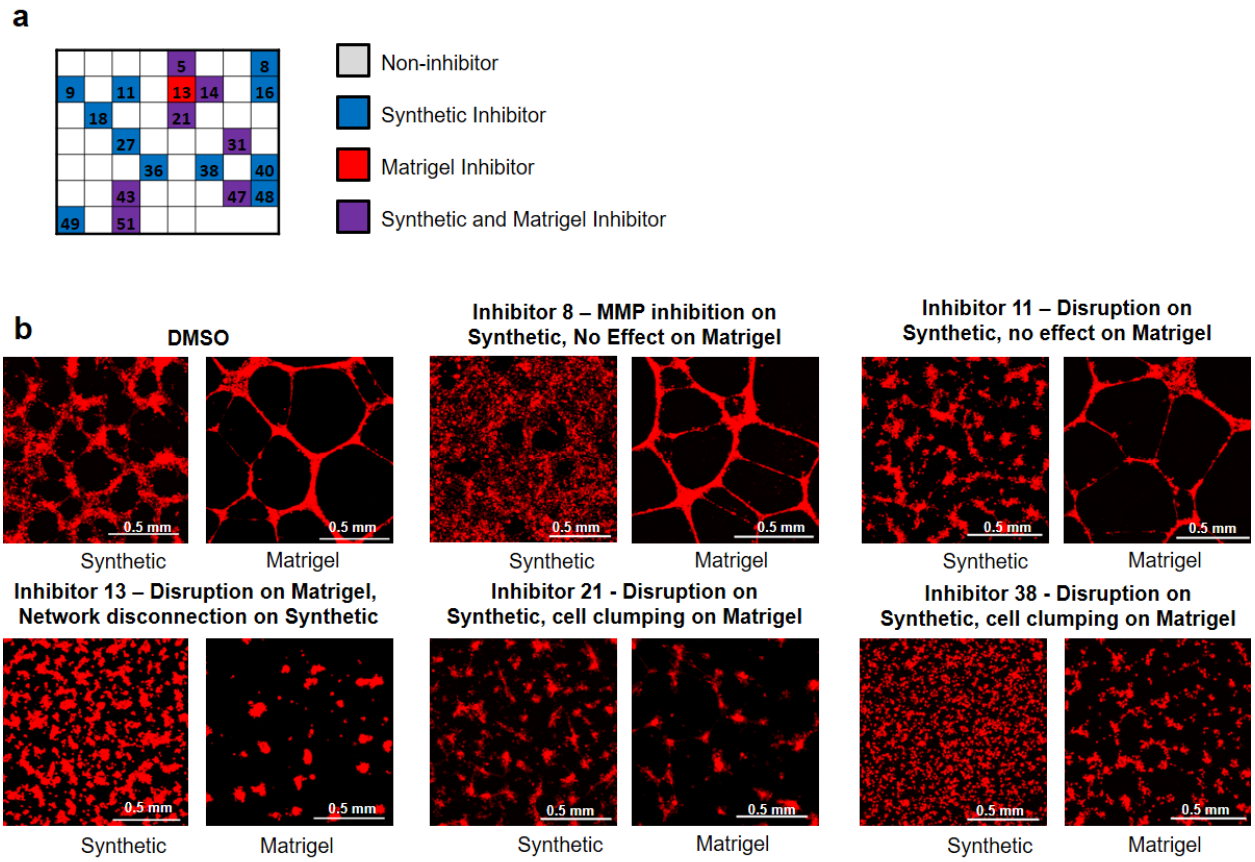


**Supplemental Figure 11** Examples of compounds identified as inhibitors by either the synthetic or Matrigel systems but not in both systems. **(A)** Inhibitors in the blinded sample matrix of 38 compounds identified on synthetic hydrogels, Matrigel, or both materials. **(B)** Sample images highlighting differential effects of inhibitors on synthetic hydrogels and Matrigel. Red: Cell Tracker Red.

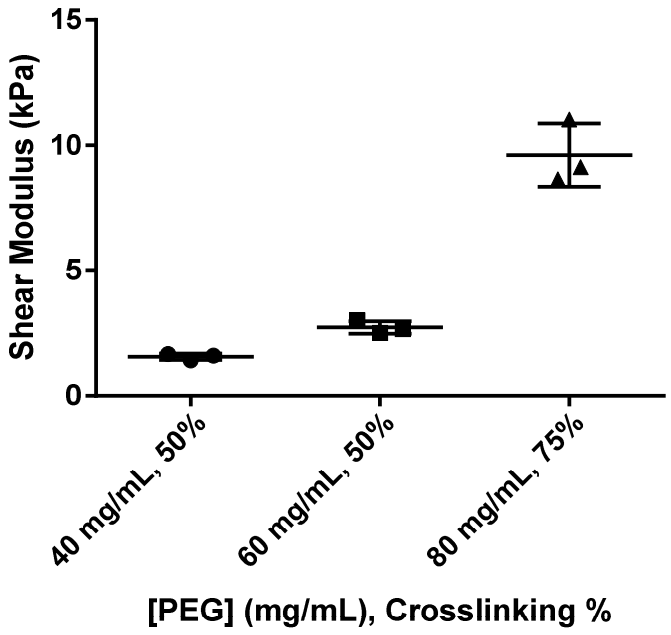


**Supplemental Figure 12** Shear modulus of synthetic hydrogels used in hESC culture. Variables included 20 kDa PEG concentration and crosslinking percentage by 3.4 kDa dithiolated PEG crosslinking molecules in the precursor solutions (n = 3). Data represents means and error bars represent standard deviations. This characterization was performed once over the course of these studies.

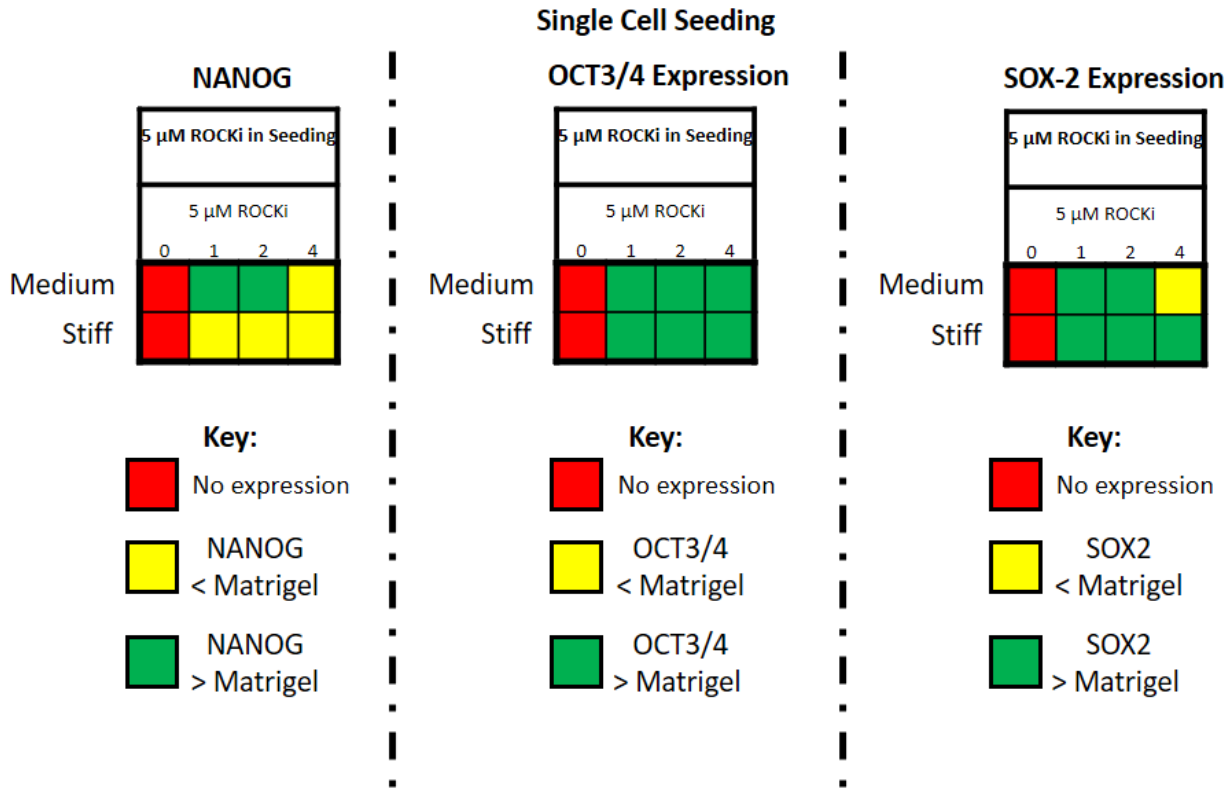


**Supplemental Figure 13** Material-dependent maintenance of hESC pluripotency. Quantitative heat map of hESC NANOG, OCT3/4 and SOX-2 expression in a subset of synthetic hydrogel-based culture conditions screened in Figure 5. (n=3, n=5 in colony seeding conditions where ROCK inhibitor was removed, n=10 in single-cell seeding conditions where ROCK inhibitor was removed). Cells were cultured with either 0 or 5 µM ROCK inhibitor in maintenance culture, and hydrogels contained 0, 1, 2 or 4 mM cyclic RGD. The screen was performed once over the course of these studies.

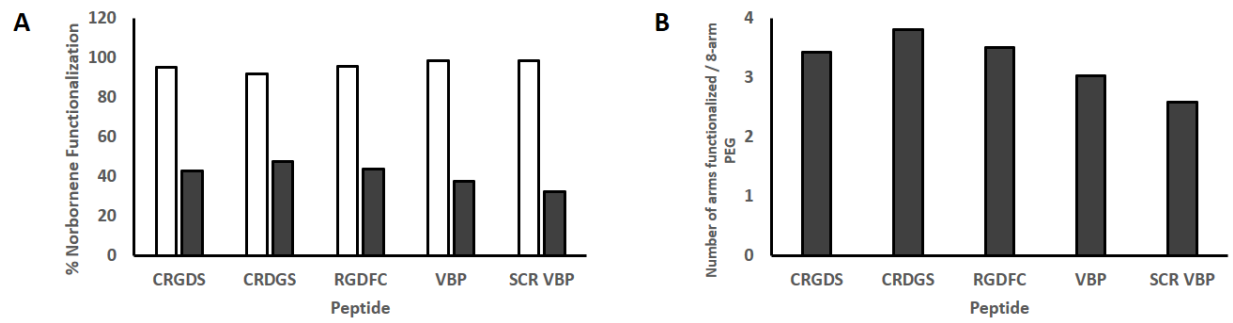


**Supplemental Figure 14** NMR quantification of peptide conjugation to PEG molecules, as performed after each conjugation reaction. **(A)** Functionalization of available PEG arms with norbornene groups was quantified through integration of proton peaks between 6.8-7.2 PPM, representing alkene protons present on a norbornene ring. After conjugation with a peptide, a reduction in alkene protons is seen, indicating that norbornene groups have been consumed by the thiol-ene reaction (n = 1 per characterization). **(B)** The number of arms of each PEG molecule is calculated through the difference between the % norbornene molecule functionalization of unreacted and reacted PEG molecules (n = 1 per characterization).

**References**


1 Jia, J. *et al.* Development of peptide-functionalized synthetic hydrogel microarrays for stem cell and tissue engineering applications. *Acta Biomater* **45**, 110-120, doi:10.1016/j.actbio.2016.09.006 (2016).

2 Jongpaiboonkit, L., King, W. J. & Murphy, W. L. Screening for 3D environments that support human mesenchymal stem cell viability using hydrogel arrays. *Tissue Eng Part A* **15**, 343-353, doi:10.1089/ten.tea.2008.0096 (2009).

3 Ranga, A. *et al.* Neural tube morphogenesis in synthetic 3D microenvironments. *Proc Natl Acad Sci U S A* **113**, E6831-E6839, doi:10.1073/pnas.1603529113 (2016).

4 Gobaa, S. *et al.* Artificial niche microarrays for probing single stem cell fate in high throughput. *Nat Methods* **8**, 949-955, doi:10.1038/nmeth.1732 (2011).

5 Ranga, A. *et al.* 3D niche microarrays for systems-level analyses of cell fate. *Nat Commun* **5**, 4324, doi:10.1038/ncomms5324 (2014).

6 Jongpaiboonkit, L., King, W. J. & Murphy, W. L. Screening for 3D Environments That Support Human Mesenchymal Stem Cell Viability Using Hydrogel Arrays. *Tissue Engineering Part A* **15**, 343-353 (2009).

7 Caiazzo, M. *et al.* Defined three-dimensional microenvironments boost induction of pluripotency. *Nat Mater* **15**, 344-352, doi:10.1038/nmat4536 (2016).

8 Jia, W. *et al.* Direct 3D bioprinting of perfusable vascular constructs using a blend bioink. *Biomaterials* **106**, 58-68, doi:10.1016/j.biomaterials.2016.07.038 (2016).

9 Zhang, Y., Xiang, Q., Dong, S., Li, C. & Zhou, Y. Fabrication and characterization of a recombinant fibronectin/cadherin bio-inspired ceramic surface and its influence on adhesion and ossification in vitro. *Acta Biomater* **6**, 776-785, doi:10.1016/j.actbio.2009.08.025 (2010).

10 Patel, A. K. *et al.* A defined synthetic substrate for serum-free culture of human stem cell derived cardiomyocytes with improved functional maturity identified using combinatorial materials microarrays. *Biomaterials* **61**, 257-265, doi:10.1016/j.biomaterials.2015.05.019 (2015).

11 Mei, Y. *et al.* Combinatorial development of biomaterials for clonal growth of human pluripotent stem cells. *Nat Mater* **9**, 768-778, doi:10.1038/nmat2812 (2010).

12 Anderson, D. G., Levenberg, S. & Langer, R. Nanoliter-scale synthesis of arrayed biomaterials and application to human embryonic stem cells. *Nat Biotechnol* **22**, 863-866, doi:10.1038/nbt981 (2004).

13 Hook, A. L. *et al.* Polymers with hydro-responsive topography identified using high throughput AFM of an acrylate microarray. *Soft Matter* **7**, 7194-7197, doi:10.1039/C1SM06063E (2011).

14 Celiz, A. D. *et al.* Discovery of a Novel Polymer for Human Pluripotent Stem Cell Expansion and Multilineage Differentiation. *Adv Mater* **27**, 4006-4012, doi:10.1002/adma.201501351 (2015).

15 Khan, F., Tare, R. S., Kanczler, J. M., Oreffo, R. O. & Bradley, M. Strategies for cell manipulation and skeletal tissue engineering using high-throughput polymer blend formulation and microarray techniques. *Biomaterials* **31**, 2216-2228, doi:10.1016/j.biomaterials.2009.11.101 (2010).

16 Jongpaiboonkit, L. *et al.* An adaptable hydrogel array format for 3-dimensional cell culture and analysis. *Biomaterials* **29**, 3346-3356 (2008).

17 Schwartz, M. P. *et al.* Human pluripotent stem cell-derived neural constructs for predicting neural toxicity. *Proc Natl Acad Sci U S A* **112**, 12516-12521, doi:10.1073/pnas.1516645112 (2015).

18 Musah, S. *et al.* Substratum-induced differentiation of human pluripotent stem cells reveals the coactivator YAP is a potent regulator of neuronal specification. *Proceedings of the National Academy of Sciences of the United States of America* **111**, 13805-13810, doi:10.1073/pnas.1415330111 (2014).

19 Pellett, S. *et al.* Human Induced Pluripotent Stem Cell Derived Neuronal Cells Cultured on Chemically-Defined Hydrogels for Sensitive In Vitro Detection of Botulinum Neurotoxin. *Scientific Reports* **5**, doi:Artn 1456610.1038/Srep14566 (2015).

20 Nguyen, E. H., Zanotelli, M. R., Schwartz, M. P. & Murphy, W. L. Differential effects of cell adhesion, modulus and VEGFR-2 inhibition on capillary network formation in synthetic hydrogel arrays. *Biomaterials* **35**, 2149-2161, doi:10.1016/j.biomaterials.2013.11.054 (2014).

21 Zanotelli, M. R. *et al.* Stable engineered vascular networks from human induced pluripotent stem cell-derived endothelial cells cultured in synthetic hydrogels. *Acta Biomater* **35**, 32-41, doi:10.1016/j.actbio.2016.03.001 (2016).

22 Qiao, S., Fei, L., Liulin, Y., Zhiqiang, W. & Xi, Z. Supramolecular polymers synthesized by thiol– ene click polymerization from supramonomers *Polymer Chemistry* **6**, 369-372 (2015).

23 Andrew, L. Thiol-ene ‘‘click’’ reactions and recent applications in polymer and materials synthesis. *Polymer Chemistry* **1**, 17-36 (2009).

24 Fairbanks, B. D. *et al.* A Versatile Synthetic Extracellular Matrix Mimic via Thiol-Norbornene Photopolymerization. *Advanced Materials* **21**, 5005-5010 (2009).

25 Hoyle, C. E. & Bowman, C. N. Thiol-ene click chemistry. *Angew Chem Int Ed Engl* **49**, 1540-1573, doi:10.1002/anie.200903924 (2010).

26 Shih, H. & Lin, C. C. Cross-linking and degradation of step-growth hydrogels formed by thiol-ene photoclick chemistry. *Biomacromolecules* **13**, 2003-2012, doi:10.1021/bm300752j (2012).

27 King, W. J., Jongpaiboonkit, L. & Murphy, W. L. Influence of FGF2 and PEG hydrogel matrix properties on hMSC viability and spreading. *Journal of Biomedical Materials Research Part A* **93A**, 1110-1123 (2010).

28 Lutolf, M. P. & Hubbell, J. A. Synthesis and physicochemical characterization of end-linked poly(ethylene glycol)-co-peptide hydrogels formed by Michael-type addition. *Biomacromolecules* **4**, 713-722 (2003).

29 Raeber, G. P., Lutolf, M. P. & Hubbell, J. A. Molecularly engineered PEG hydrogels: A novel model system for proteolytically mediated cell migration. *Biophysical Journal* **89**, 1374-1388 (2005).

30 Toepke, M., Impellitteri, N., JM, T. & WL, M. Characterization of Thiol-Ene Crosslinked PEG Hydrogels. *Macromolecular Materials and Engineering* **10.1002/mame.201200119** (2012).

31 Wood, J. M. *et al.* PTK787/ZK 222584, a novel and potent inhibitor of vascular endothelial growth factor receptor tyrosine kinases, impairs vascular endothelial growth factor-induced responses and tumor growth after oral administration. *Cancer Res* **60**, 2178-2189 (2000).

32 Latham, A. M. *et al.* Indolinones and anilinophthalazines differentially target VEGF-A- and basic fibroblast growth factor-mediated responses in primary human endothelial cells. *Br J Pharmacol* **165**, 245-259, doi:10.1111/j.1476-5381.2011.01545.x (2012).

33 Friis, T., Engel, A. M., Bendiksen, C. D., Larsen, L. S. & Houen, G. Influence of levamisole and other angiogenesis inhibitors on angiogenesis and endothelial cell morphology in vitro. *Cancers (Basel)* **5**, 762-785, doi:10.3390/cancers5030762 (2013).

34 Sarkanen, J. R. *et al.* Intra-Laboratory Pre-Validation of a Human Cell Based in vitro Angiogenesis Assay for Testing Angiogenesis Modulators. *Front Pharmacol* **1**, 147, doi:10.3389/fphar.2010.00147 (2010).

35 Friis, T., Hansen, A. B., Houen, G. & Engel, A. M. Influence of angiogenesis inhibitors on endothelial cell morphology in vitro. *APMIS* **114**, 211-224, doi:10.1111/j.1600-0463.2006.apm_189.x (2006).

36 Sims, T. L. *et al.* Bevacizumab suppresses neuroblastoma progression in the setting of minimal disease. *Surgery* **144**, 269-275, doi:10.1016/j.surg.2008.04.009 (2008).

37 Brossa, A. *et al.* Sunitinib but not VEGF blockade inhibits cancer stem cell endothelial differentiation. *Oncotarget* **6**, 11295-11309, doi:10.18632/oncotarget.3123 (2015).

38 Enemchukwu, N. O. *et al.* Synthetic matrices reveal contributions of ECM biophysical and biochemical properties to epithelial morphogenesis. *J Cell Biol* **212**, 113-124, doi:10.1083/jcb.201506055 (2016).

39 Gjorevski, N. *et al.* Designer matrices for intestinal stem cell and organoid culture. *Nature* **539**, 560-564, doi:10.1038/nature20168 (2016).

40 Bott, K. *et al.* The effect of matrix characteristics on fibroblast proliferation in 3D gels. *Biomaterials* **31**, 8454-8464, doi:10.1016/j.biomaterials.2010.07.046 (2010).

41 Raeber, G. P., Lutolf, M. P. & Hubbell, J. A. Mechanisms of 3-D migration and matrix remodeling of fibroblasts within artificial ECMs. *Acta Biomaterialia* **3**, 615-629 (2007).

42 Ehrbar, M. *et al.* Enzymatic formation of modular cell-instructive fibrin analogs for tissue engineering. *Biomaterials* **28**, 3856-3866 (2007).

43 Ehrbar, M. *et al.* Biomolecular hydrogels formed and degraded via site-specific enzymatic reactions. *Biomacromolecules* **8**, 3000-3007, doi:10.1021/bm070228f (2007).

44 Hansen, T. D. *et al.* Biomaterial arrays with defined adhesion ligand densities and matrix stiffness identify distinct phenotypes for tumorigenic and non-tumorigenic human mesenchymal cell types. *Biomaterials Science* **2**, 745-756, doi:10.1039/c3bm60278h (2014).

45 Le, N. N. T., Zorn, S., Schmitt, S. K., Gopalan, P. & Murphy, W. L. Hydrogel arrays formed via differential wettability patterning enable combinatorial screening of stem cell behavior. *Acta Biomaterialia* **34,** 93-103 (2015).

46 Belair, D. G., Le, N. N. & Murphy, W. L. Design of growth factor sequestering biomaterials. *Chem Commun (Camb)* **50**, 15651-15668, doi:10.1039/c4cc04317k (2014).

47 Belair, D. G. & Murphy, W. L. Specific VEGF sequestering to biomaterials: Influence of serum stability. *Acta Biomaterialia*, doi:10.1016/j.actbio.2013.06.033 (2013).

48 Hudalla, G. A. & Murphy, W. L. Biomaterials that regulate growth factor activity via bioinspired interactions. *Adv Funct Mater* **21**, 1754-1768, doi:10.1002/adfm.201002468 (2011).
49 Belair, D. G. & Murphy, W. L. Specific VEGF sequestering to biomaterials: influence of serum stability. *Acta Biomater* **9**, 8823-8831, doi:10.1016/j.actbio.2013.06.033 (2013).
50 Murphy, W. L., McDevitt, T. C. & Engler, A. J. Materials as stem cell regulators. *Nat Mater* **13**, 547-557, doi:10.1038/nmat3937 (2014).
51 Guzmán-Hernández, M. L., Potter, G., Egervári, K., Kiss, J. Z. & Balla, T. Secretion of VEGF-165 has unique characteristics, including shedding from the plasma membrane. *Mol Biol Cell* **25**, 1061-1072, doi:10.1091/mbc.E13-07-0418 (2014).
52 E, G. *et al.* Endogenous vascular endothelial growth factor-A (VEGF-A) maintains endothelial cell homeostasis by regulating VEGF receptor-2 transcription. *J Biol Chem* **287**, 3029-3041, doi:10.1074/jbc.M111.293985 (2012).
53 Koch, S. & Claesson-Welsh, L. Signal transduction by vascular endothelial growth factor receptors. *Cold Spring Harb Perspect Med* **2**, a006502, doi:10.1101/cshperspect.a006502 (2012).